

An Efficient Volume Integral-Equation Approach for Characterization of Lossy Dielectric Materials

Man-Leung Lui, *Student Member, IEEE*, and Ke-Li Wu, *Senior Member, IEEE*

Abstract—An efficient volume integral-equation approach for characterizing lossy dielectric materials in the Courtney holder type of measurement environment is proposed. Utilizing the parallel-plate dyadic Green's functions and the volume equivalence theorem, an effective electric-field integral equation is developed for azimuthally invariant mode analysis of a parallel-plate dielectric resonator. Volumetric cylindrical pulse basis functions and a point-matching moment-method procedure are used to formulate an eigenvalue problem. A novel singularity treatment, which uses a Bessel function identity, is presented. In an iterative permittivity searching process, perturbation of the eigenmatrix equation involves solely recomputing a diagonal matrix, which is a function of permittivity only. Therefore, the efficiency of the searching process is greatly increased. Two numerical examples are provided to illustrate the applicability and validity of the proposed approach to the evaluation of dielectric constant, loss tangent, and surface resistance of the parallel plates.

Index Terms—Complex permittivity, dielectric resonator (DR), dyadic Green's functions, method of moments (MoM), volume integral equation (VIE).

I. INTRODUCTION

CHARACTERIZATION of lossy dielectric materials is widely performed in the Courtney holder type of measurement environment where a precisely machined dielectric specimen is placed within a pair of parallel metal plates [1]–[4]. Dielectric material properties (dielectric constant and loss tangent) can then be evaluated via numerical analysis in which input parameters are the measured resonant frequency (f_0), the extracted unloaded quality factor (Q_u) from the measured loaded quality factor (Q_L), and the measured physical dimensions of the entire resonator system. Different numerical approaches such as the finite-element method (FEM), frequency-domain finite-difference (FDFD) method, and mode-matching (MM) method can be used to carry out such analysis [1]. For the volumetric-discretization-based techniques such as FEM and FDFD approaches, re-solving a large sparse matrix equation repeatedly is always needed when the permittivity value is the search parameter. This is a very time-consuming process. Unlike the FDFD and FEM approaches, the MM approach does not generate a large matrix system. However, the permittivity searching routine also requires re-solving the entire eigenvalue problem repeatedly. Therefore, a lookup table is usually prepared by performing sufficient pre-calculations.

In this paper, an efficient volume integral-equation (VIE) approach is presented for characterizing lossy dielectric materials in the Courtney holder type of measurement environment, in which neither a large matrix system, nor an entire eigenvalue problem needs to be resolved in an iterative permittivity

searching process. Utilizing the parallel-plate dyadic Green's functions (PP DGFs) [5] and the volume equivalence theorem (VET) [6], an effective volume electric field integral equation (EFIE) is developed for characterizing a parallel-plate dielectric resonator (DR). The volumetric cylindrical pulse basis functions (VCPBFs) and a point-matching method-of-moments (PM MoM) procedure are used to formulate the eigenvalue problem. The formulated eigenvalue matrix, in general, consists of a moderately sparse impedance matrix and diagonal matrix. While the impedance matrix is a function of frequency and physical dimensions of the resonator system, the diagonal matrix is a function of the DR's permittivity only. As the filling of the impedance matrix is required only once for a given resonant frequency, the workload of the search is mainly contributed by computing the matrix's determinant using the singular-value-decomposition (SVD) algorithm [7] after the diagonal matrix is updated for each permittivity trial. This feature makes the proposed VIE approach very efficient for dielectric material characterization using the Courtney method [1]–[4].

Despite the merits of employing the PP DGF in the VIE formulation, much attention must be paid to the singularity treatments, as they are vital in the VIE implementation. The formulated volume EFIE is simplified solely for the analysis of rotationally symmetric modes due to their practicality in the Courtney's measurement procedure [1]–[4]. Hence, the consideration in the treatments of the singular integral equations is down to five dyadic components only, namely, the $\hat{r}\hat{r}$, $\hat{r}\hat{z}$, $\hat{\phi}\hat{\phi}$, $\hat{z}\hat{r}$, and $\hat{z}\hat{z}$ components. In general, the singularity treatments for the five singular integrals are different; however, only the novel treatment for the $\hat{z}\hat{r}$ dyad component is discussed, in which a Bessel function identity is used to facilitate the singularity extraction. With the extracted logarithmic singularity being properly addressed, the inherited slow convergence behavior (oscillatory in nature) associated with the self-coupling term in the impedance matrix is removed. The final expressions after applying the singularity treatments for all singular integral equations are given in the Appendix. The numerical analysis of rod- and ring-shaped parallel-plate lossy DRs shows the validation of the singularity treatments. Two numerical examples are given to demonstrate the applicability and validity of the proposed approach: one is the evaluation of the dielectric constant ϵ_r , which is based on experimental results and the other one is the characterization of dielectric post and the surface resistance R_s of the parallel plates, which is based on the measurement data available in the literature [8] using so-called "two-resonator method." The computed characteristics agree well with those obtained by the commercial software Ansoft High Frequency Structure Simulator (HFSS) or the analytical solutions available from literature. In the following discussion, the complex number $\dot{j} = \sqrt{-1}$ is used and the time dependence of $e^{-j\omega t}$ is assumed and suppressed.

Manuscript received July 30, 2004.

The authors are with the Department of Electronic Engineering, The Chinese University of Hong Kong, Satin, Hong Kong (e-mail: klwu@ee.cuhk.edu.hk).
Digital Object Identifier 10.1109/TMTT.2004.837149

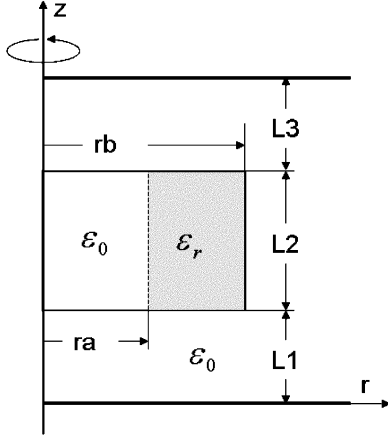


Fig. 1. Parallel-plate DR configuration.

II. VIE FORMULATION

Consider a boundary value problem, in which a linear, homogeneous, and isotropic DR specimen is placed between a parallel-plate waveguide, as depicted in Fig. 1. The VIE formulation begins with the employment of VET [6, p. 224] that the electric-field intensity within the DR can be expressed as

$$\vec{E}(\vec{R}) = \frac{\vec{J}_{\text{eq}}(\vec{R})}{-j\omega\epsilon_0(\epsilon_r - 1)} \quad (1)$$

where ϵ_r is the relative permittivity of the DR specimen and can be complex for a lossy case. The formulated volume EFIE with the PP-DGF kernel [5] $\vec{G}_{e1}(\vec{R}, \vec{R}')$ for the described problem is

$$\frac{\vec{J}_{\text{eq}}(\vec{R})}{-j\omega\epsilon_0(\epsilon_r - 1)} = \frac{1}{j\omega\epsilon_0} \vec{J}_{\text{eq},r}(\vec{R}) + j\omega\mu_0 \int_{v'} \text{p.v.} \vec{G}_{e1}(\vec{R}, \vec{R}') \cdot \vec{J}_{\text{eq}}(\vec{R}') dv' \quad (2)$$

where p.v. denotes the principal value portion of the PP DGF. For the analysis of rotationally symmetric modes, the inner product for the p.v. $\vec{G}_{e1}(\vec{R}, \vec{R}')$ with the equivalent current density $\vec{J}_{\text{eq}}(\vec{R}')$ in (2) is

$$\text{p.v.} \vec{G}_{e1}(\vec{R}, \vec{R}') \cdot \vec{J}_{\text{eq}}(\vec{R}') = \begin{bmatrix} G_{e1,0}^{rr}(\vec{R}, \vec{R}') & 0 & G_{e1,0}^{rz}(\vec{R}, \vec{R}') \\ 0 & G_{e1,0}^{\phi\phi}(\vec{R}, \vec{R}') & 0 \\ G_{e1,0}^{zr}(\vec{R}, \vec{R}') & 0 & G_{e1,0}^{zz}(\vec{R}, \vec{R}') \end{bmatrix} \cdot \begin{bmatrix} J_{\text{eq},r}(\vec{R}') \\ J_{\text{eq},\phi}(\vec{R}') \\ J_{\text{eq},z}(\vec{R}') \end{bmatrix} \quad (3)$$

where each dyad component is an eigenfunction series summation, e.g.,

$$G_{e1,0}^{zr}(\vec{R}, \vec{R}') = \frac{-j}{2Lk_0^2} \cdot \sum_{m=1}^{\infty} \left(\left\{ \begin{aligned} & H_0^{(1)}(k_r r) \cdot J_0'(k_r r') \\ & J_0(k_r r) \cdot H_0^{(1)'}(k_r r') \end{aligned} \right\} \cdot k_z \cdot k_r \cdot \cos(k_z z) \cdot \sin(k_z z') \right), \quad (4)$$

for $\begin{cases} r > r' \\ r < r' \end{cases}$.

In the above, subscript 0 for the five nonzero Green's function dyad components in (3) signifies that the resonant modes under consideration are ϕ independent. k_0 is the free-space wavenumber, $k_z = m\pi/L$ is the wavenumber in the axial direction, and k_r is the wavenumber in the radial direction, which is equal to $\sqrt{k_0^2 - k_z^2}$ for propagation modes and $j\sqrt{k_z^2 - k_0^2}$ for evanescent modes. Both $J_0'(k_r r')$ and $H_0^{(1)'}(k_r r')$ in (4) are spatial derivatives with respect to the argument $k_r r'$. As can be seen from (3), both the \hat{r} - and \hat{z} -directed electric-field intensities are independent of the $\hat{\phi}$ -directed current density, while the $\hat{\phi}$ -directed electric-field intensity depends only on the $\hat{\phi}$ -directed current density.

The equivalent current density $\vec{J}_{\text{eq}}(\vec{R}')$ in (2) can be approximated by a set of finite series using VCPBFs, i.e.,

$$\vec{J}_{\text{eq}}(\vec{R}') \approx \sum_{k=1}^K \bar{a}_{\text{eq},k} \cdot \vec{J}_{\text{eq},k}(\vec{R}') = \sum_{k=1}^K \begin{bmatrix} a_{\text{eq},r,k} \cdot J_{\text{eq},r,k}(\vec{R}') \\ a_{\text{eq},\phi,k} \cdot J_{\text{eq},\phi,k}(\vec{R}') \\ a_{\text{eq},z,k} \cdot J_{\text{eq},z,k}(\vec{R}') \end{bmatrix} \quad (5)$$

where $\bar{a}_{\text{eq},k}$ is the k th unknown coefficient array to be determined by a set of $3K$ simultaneous linear equations. $\vec{J}_{\text{eq},k}(\vec{R}')$ represents the k th VCPBF term and is defined as

$$J_{\text{eq},i,k}(\vec{R}') = \begin{cases} 1, & \text{for } \vec{R}' \in \Delta V_k \text{ or } r'_k - \frac{\Delta r'}{2} \leq r' \leq r'_k + \frac{\Delta r'}{2}, \\ 0, & \text{for } \vec{R}' \notin \Delta V_k \text{ or } z'_k - \frac{\Delta z'}{2} \leq z' \leq z'_k + \frac{\Delta z'}{2} \\ & \text{elsewhere} \end{cases} \quad (6)$$

where $i = r, \phi, \text{ or } z$. Generally, ΔV_k is a doughnut-shaped volume cell. However, $r'_k - (\Delta r'/2)$ can be zero in the case of a solid DR.

In order to extract the singularity, $\vec{G}_{e1}(\vec{R}, \vec{R}')$ can be written as

$$\vec{G}_{e1}(\vec{R}, \vec{R}') = \left\{ \vec{G}_{e1}(\vec{R}, \vec{R}') - \vec{G}_a(\vec{R}, \vec{R}') \right\} + \vec{G}_a(\vec{R}, \vec{R}'). \quad (7)$$

In (7), $\vec{G}_a(\vec{R}, \vec{R}')$ is the asymptotic form of $\vec{G}_{e1}(\vec{R}, \vec{R}')$ in which the Bessel functions are replaced by their corresponding

large argument asymptotic expressions. Defining the ϕ -invariant weighting function array as

$$\vec{w}_q = \frac{1}{2\pi r} \delta(r - r_q) \delta(z - z_q) [1 \quad 1 \quad 1]^T \quad (8)$$

where q and T are the observation location index and transpose operator, respectively. Substituting (5) into (2) and applying the point-matching procedure give the following eigenmatrix equation:

$$[\vec{A}] [\vec{a}_{\text{eq}}] = k_0^2 \left([\vec{B}] + [\vec{C}] \right) [\vec{a}_{\text{eq}}] \quad (9)$$

where

$$\vec{A}_{qk} = \frac{\delta_{qk}}{\varepsilon_r(\vec{R}_q) - 1} \begin{bmatrix} \varepsilon_r(\vec{R}_q) & 0 & 0 \\ 0 & 1 & 0 \\ 0 & 0 & 1 \end{bmatrix} \quad (10)$$

$$\vec{B}_{qk} = 2\pi \int_{z'_k - \frac{\Delta z'}{2}}^{z'_k + \frac{\Delta z'}{2}} \int_{r'_k - \frac{\Delta r'}{2}}^{r'_k + \frac{\Delta r'}{2}} \vec{G}_{e1}(\vec{R}_q, \vec{R}') - \vec{G}_a(\vec{R}_q, \vec{R}') r' dr' dz' \quad (11)$$

and

$$\vec{C}_{qk} = 2\pi \int_{z'_k - \frac{\Delta z'}{2}}^{z'_k + \frac{\Delta z'}{2}} \int_{r'_k - \frac{\Delta r'}{2}}^{r'_k + \frac{\Delta r'}{2}} \vec{G}_a(\vec{R}_q, \vec{R}') r' dr' dz'. \quad (12)$$

In (10), δ_{qk} is the Kronecker delta function. Obviously, $[\vec{A}]$ is a diagonal matrix and is the only matrix that is a function of ε_r among the three matrices in (9). In (11) and (12), p.v. associated with the PP DGF is dropped for simplicity. With the subtraction of $\vec{G}_a(\vec{R}_q, \vec{R}')$ in (11), the eigenfunction summations associated with the Green's function series in the evaluation of the self-coupling terms of the impedance matrix now converges. In order to handle the integrable singular integrand in the $\hat{z}\hat{r}$ component of (12), the inherited logarithmic singularity must be treated as discussed in Section III.

III. SINGULARITY TREATMENT FOR THE $\hat{z}\hat{r}$ DYAD [9]

In order to facilitate the singularity extraction for the $\hat{z}\hat{r}$ dyad component, the following Bessel function identity is used:

$$B_0(k_r r) = - \left[\frac{d}{dr} + \frac{1}{r} \right] \left(\frac{B'_0(k_r r)}{k_r} \right) \quad (13)$$

where $B_0(k_r r)$ can be $J_0(k_r r)$ or $H_0^{(1)}(k_r r)$. Having replaced the Bessel functions $J_0(k_r r)$ and $H_0^{(1)}(k_r r)$ in (4) with their corresponding Bessel function identity in (13), the m th term of (4) ($G_{e1,0m}^{zr}$) becomes

$$G_{e1,0m}^{zr} = \frac{-j}{2Lk_0^2} \left[\frac{d}{dr} + \frac{1}{r} \right] \left[\frac{-1}{k_r} \left\{ \begin{array}{l} H_0^{(1)'}(k_r r) \\ J_0'(k_r r) \end{array} \right\} k_z \cos k_z z \right] \cdot \left[\left\{ \begin{array}{l} J_0(k_r r') \\ H_0^{(1)'}(k_r r') \end{array} \right\} k_r \sin k_z z' \right], \quad \text{for } \begin{cases} r > r' \\ r < r' \end{cases} \quad (14)$$

and its corresponding asymptotic expression form becomes

$$G_{a,0m}^{zr} = \frac{1}{L\pi k_0^2} \left[\frac{d}{dr} + \frac{1}{r} \right] \left[\frac{1}{\sqrt{r}} \left\{ \begin{array}{l} e^{j(k_z r - \frac{3}{4}\pi)} \\ \cos \left(jk_z r - \frac{3}{4}\pi \right) \end{array} \right\} \cos k_z z \right] \cdot \left[\frac{1}{\sqrt{r'}} \left\{ \begin{array}{l} \cos \left(jk_z r' - \frac{3}{4}\pi \right) \\ e^{j(k_z r' - \frac{3}{4}\pi)} \end{array} \right\} \sin k_z z' \right], \quad \text{for } \begin{cases} r > r' \\ r < r' \end{cases} \quad (15)$$

Expressing all the cosine terms with the r and r' variables in (15) into their exponential equivalence gives

$$G_{a,0m}^{zr} = \frac{1}{L\pi k_0^2} \left(\frac{1}{r} \xi(r, r', z, z') + \frac{d}{dr} \xi(r, r', z, z') \right) \quad (16)$$

where

$$\xi(r, r', z, z') = \frac{1}{2\sqrt{rr'}} \left\{ \begin{array}{l} e^{-k_z(r+r') - j\frac{3}{2}\pi} + e^{-k_z(r-r')} \\ e^{-k_z(r+r') - j\frac{3}{2}\pi} + e^{-k_z(r'-r)} \end{array} \right\} \times (\cos(k_z z) \sin(k_z z')), \quad \text{for } \begin{cases} r > r' \\ r < r' \end{cases} \quad (17)$$

Now, $G_{e1,0m}^{zr}$ can be represented as a continuous expression in which

$$\xi(r, r', z, z') = \frac{1}{4\sqrt{rr'}} \left(e^{-k_z|r+r'| - j\frac{3}{2}\pi} + e^{-k_z|r-r'|} \right) \times (\sin k_z(z+z') - \sin k_z(z-z')). \quad (18)$$

In the algebraic manipulation from (17) to (18), the products of cosine and sine functions with variables z and z' have been expressed in terms of sine functions only. This is done so that the closed-form sum of (18) can be found after performing an analytical integration with respect to the z' variable in the PM-MoM procedure.

Having introduced the Bessel function identity in the singularity extraction, the strong type ($\sim 1/R^3$) singular $\hat{z}\hat{r}$ Green's function is now split into two terms in which its singularity can be easily handled by the classical technique. On the right-hand side of (16), the first term is of a weaker type ($\sim 1/R^2$) singularity because of the $1/k_r$ term introduced in the Bessel function identity. Hence, the volume integration can ensure the convergence of the series summation. The second term is of a strong type singularity because of the d/dr derivative. Nevertheless, the singularity can be dealt with by rearranging the order of derivative and integration in the integro-differential equation with the assumption of satisfaction of the Hölder condition [6, p. 231] for the equivalent current density \vec{J}_{eq} . Despite some tedious algebraic manipulation, the following volume integral expression (before carrying out the inner product with the weighting function) can be obtained:

$$2\pi \int_{z'_k - \frac{\Delta z'}{2}}^{z'_k + \frac{\Delta z'}{2}} \int_{r'_k - \frac{\Delta r'}{2}}^{r'_k + \frac{\Delta r'}{2}} \left(\sum_m G_{a,0m}^{zr}(\vec{R}, \vec{R}') \right) r' dr' dz'$$

$$\begin{aligned}
&= \frac{1}{r} \left(2\pi \int_{z'_k - \frac{\Delta z'}{2}}^{z'_k + \frac{\Delta z'}{2}} \int_{r'_k - \frac{\Delta r'}{2}}^{r'_k + \frac{\Delta r'}{2}} \sum_m \xi(r, r', z, z') r' dr' dz' \right) \\
&+ \frac{d}{dr} \left(2\pi \int_{z'_k - \frac{\Delta z'}{2}}^{z'_k + \frac{\Delta z'}{2}} \int_{r'_k - \frac{\Delta r'}{2}}^{r'_k + \frac{\Delta r'}{2}} \sum_m \xi(r, r', z, z') r' dr' dz' \right) \quad (19)
\end{aligned}$$

where

$$\begin{aligned}
&2\pi \int_{z'_k - \frac{\Delta z'}{2}}^{z'_k + \frac{\Delta z'}{2}} \int_{r'_k - \frac{\Delta r'}{2}}^{r'_k + \frac{\Delta r'}{2}} \sum_m \xi(r, r', z, z') r' dr' dz' \\
&= \frac{1}{2L} \sum_{m=1}^{\infty} \left(\int_{r'_k - \frac{\Delta r'}{2}}^{r'_k + \frac{\Delta r'}{2}} \left(e^{-k_z |r+r'| - j\frac{3}{2}\pi} + e^{-k_z |r-r'|} \right) \sqrt{\frac{r}{r'}} dr' \right. \\
&\quad \cdot \frac{1}{k_z} \left(\cos(k_z z_{t2}) - \cos(k_z z_{t1}) \right. \\
&\quad \quad \left. \left. - \cos(k_z z_{t3}) + \cos(k_z z_{t4}) \right) \right) \quad (20)
\end{aligned}$$

or

$$\begin{aligned}
&= \frac{-1}{4\pi k_0^2} \\
&\cdot \int_{r'_k - \frac{\Delta r'}{2}}^{r'_k + \frac{\Delta r'}{2}} \sqrt{\frac{r'}{r}} \left(e^{-j\frac{3}{2}\pi} \log_e \left[\frac{F_1(r+r', z_{t2}) \cdot F_1(r+r', z_{t4})}{F_1(r+r', z_{t1}) \cdot F_1(r+r', z_{t3})} \right] \right. \\
&\quad \left. + \log_e \left[\frac{F_1(|r-r'|, z_{t2}) \cdot F_1(|r-r'|, z_{t4})}{F_1(|r-r'|, z_{t1}) \cdot F_1(|r-r'|, z_{t3})} \right] \right) dr'. \quad (21)
\end{aligned}$$

In (21), $F_1(r, z) = 1 - 2e^{-(\pi/L)r} \cos(z) + e^{-2(\pi/L)r}$, $z_{t1} = z + z'_k + (\Delta z_k/2)$, $z_{t2} = z + z'_k - (\Delta z_k/2)$, $z_{t3} = z - z'_k - (\Delta z_k/2)$, and $z_{t4} = z - z'_k + (\Delta z_k/2)$. The summation expression $\sum_{m=1}^{\infty} (e^{-m\alpha}/m) \cos(m\beta) = -(1/2) \log_e(1 - 2e^{-\alpha} \cos(\beta) + e^{-2\alpha})$ is also used in deriving (21) from (20). Although only the treatment for the $\hat{z}\hat{r}$ component is fully described here, the other four nonzero dyad components ($\hat{r}\hat{r}$, $\hat{r}\hat{z}$, $\hat{\phi}\hat{\phi}$, and $\hat{z}\hat{z}$) can be handled in a similar or classical manner. The expressions of all five dyad components for the self-coupling term evaluations are presented in the Appendix.

IV. NUMERICAL CONVERGENCE

In general, the parameters that affect the convergence rate of the MoM solution are the step size ($N_{\Delta r'}$) of the numerical integration with respect to the source variable r' , the mesh (or grid) size ($\Delta r'$ and $\Delta z'$) of the discretized dielectric specimen, and the truncated number of summation terms (M_G) in approximating the Green's function. In the actual numerical implementation, all the spatial integrations in their final forms with respect to the source variable r' are numerically evaluated, as the closed-form integral cannot be obtained at the moment. In

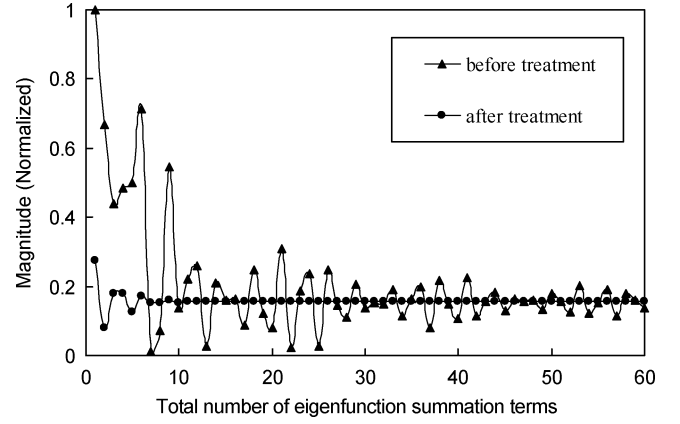


Fig. 2. Typical convergence behavior for the self-coupling term evaluation of the $\hat{z}\hat{r}$ dyad element “before” and “after” applying the singularity treatment for a ring-shaped DR.

general, computation of the double integral in (11) and (12) for each dyad component is a three-dimensional (3-D) summation process. While two are due to the numerical integrations with respect to the r' and z' variables, one is due to the series summation of the Green's function. However, analytical integration with respect to the z' variable can always be found for all five dyad components. Hence, the summation process is usually of two-dimensional (2-D) and sometimes even one-dimensional (1-D) only, in which closed-form expression for the infinite series can be found. For the sake of simplicity in the numerical implementation, the number of meshes in the radial direction is set equal to that in the axial direction (i.e., $M_{\Delta r'} = M_{\Delta z'}$). Also, the number of finite summation terms for the five components are all set to equal.

To validate the proposed singularity treatment, a lossy ring-shaped DR structure ($ra = 2$ mm, $rb = 3.015$ mm, $L1 = L3 = 3.4112$ mm, $L2 = 4.16$ mm, $\epsilon_r = 36$, and $\tan \delta = 1 \times 10^{-4}$) is considered. Fig. 2 illustrates a typical convergence behavior regarding the difference between “before” and “after” applying the singularity treatments for the self-coupling term evaluation of the $\hat{z}\hat{r}$ dyad element. The “before” treatment case was computed by splitting the integration into two parts (one for the condition $r > r'$ and the other for the condition $r < r'$). Hence, the integration (with respect to the source variable r') has never been carried across the observation point. The “after” treatment employs (21) in which only approximately ten terms are required to remove the oscillatory slow convergence behavior. A typical f_0 convergence for various number of Green's function summation terms ($M_G = N_{\Delta r'}$) and the number of meshes for the DR ($M_{\Delta r'} = M_{\Delta z'} = M_{\Delta}$) is shown in Table I. With the same set of dimensions (except $ra = 0$ for the case of a rod-shaped DR), both ring- and rod-shaped DRs are analyzed for their $TE_{01\delta}$ and $TE_{01(1+\delta)}$ modes. For a given range of dielectric constants ($30 \leq \epsilon_r \leq 40$), the computed f_0 and Q_u are illustrated in Figs. 3 and 4, respectively. While f_0 is determined via the SVD technique [7], Q_u is obtained using the complex resonant frequency formula $1/2 \cdot |f_{\text{real}}/f_{\text{imag}}|$ [1, p. 276]. Good agreement is observed, as the results are compared with those obtained using Ansoft HFSS.

TABLE I
CONVERGENCE FOR THE f_0 OF RING-SHAPED DR ($TE_{01(1+\delta)}$ MODE) WITH $\epsilon_r = 36$, $ra = 2$ mm, $rb = 3.015$ mm, $L1 = L3 = 3.4112$ mm, AND $L2 = 4.16$ mm

M_Δ	$M_G = 60$		$M_G = 80$	
	f_0 (GHz)	f_0 (GHz)	f_0 (GHz)	f_0 (GHz)
3	13.727	13.723		
4	13.808	13.811		
5	13.831	13.828		
6	13.837	13.834		
7	13.833	13.834		
8	13.832	13.833		
9	13.831	13.832		
10	13.829	13.829		

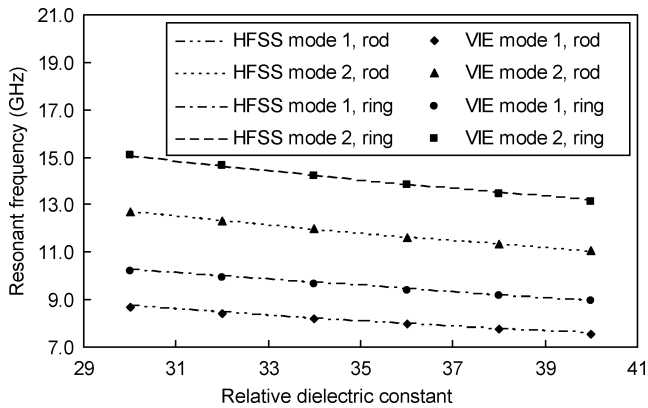


Fig. 3. Resonant frequencies of $TE_{01\delta}$ (mode 1) and $TE_{01(1+\delta)}$ (mode 2) for rod and ring DRs for various dielectric constants.

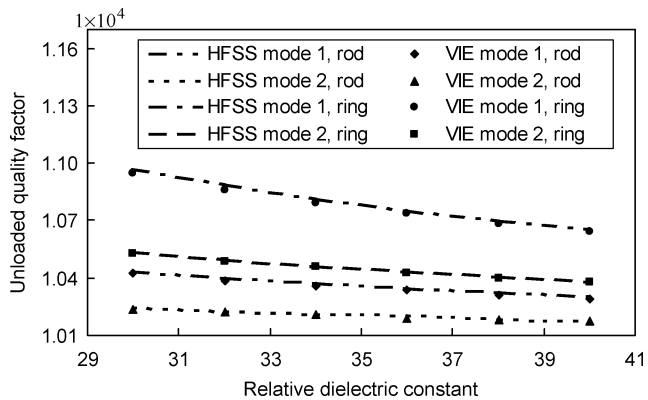


Fig. 4. Unloaded quality factors of $TE_{01\delta}$ (mode 1) and $TE_{01(1+\delta)}$ (mode 2) for rod and ring DRs for various dielectric constants.

V. NUMERICAL EXAMPLES

The first example illustrates the applicability of the proposed VIE approach in the evaluation of ϵ_r . An in-house Courtney fixture is built for the measurement. The parallel-plate fixture is made of copper (Cu) with a diameter of approximately 180 mm and is large enough for an infinite parallel-plate waveguide modeling for practical purposes. An alumina DR specimen with $\epsilon_r = \epsilon_{r1} = 9.6$, $ra = 0.0$, $rb = 6.23$ mm, and $L2 = 12.56$ mm is used in the measurement. To obtain multiple f_0 samples for the use of a single dielectric specimen, two types of parallel-plate DR configurations are considered in which type I has $L1 = L3 = 0.0$ and type II has $L1 = 0.0$ mm and

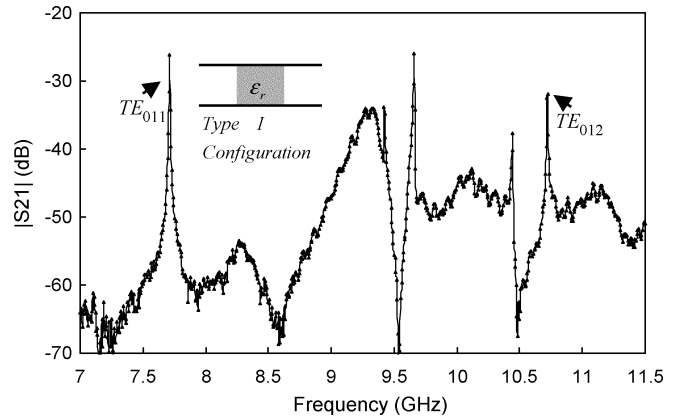


Fig. 5. Measured S_{21} response for type-I configuration.

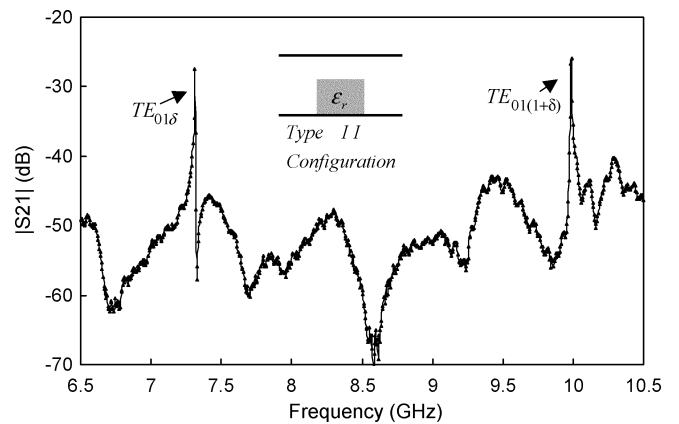


Fig. 6. Measured S_{21} response for type-II configuration.

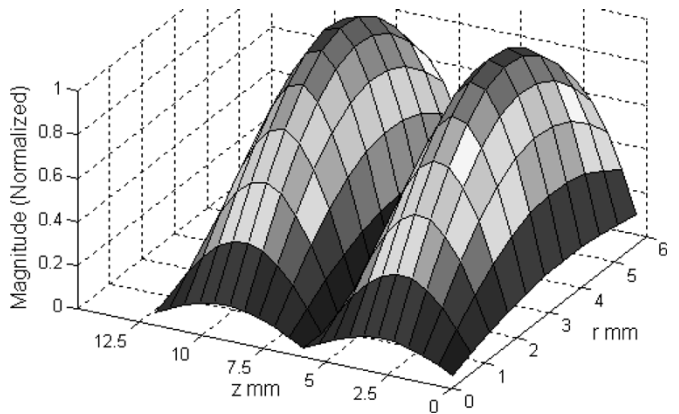


Fig. 7. Electric-field distributions on the rz -plane for the TE_{012} mode of a type-I configuration.

$L3 = 2.44$ mm. The measured S_{21} (in decibels) responses are obtained via an HP8510C network analyzer and are illustrated in Figs. 5 and 6. To confirm the identity of resonant modes, the corresponding modal field distributions can be obtained from the VIE analysis, and the TE_{012} -mode electric-field distribution for the rz -plane is shown in Fig. 7.

Despite the fact that an analytical solution is available for the type-I configuration, a numerical solution must be sought for the type-II configuration. With the measured f_0 and physical dimensions, an eigenvalue search using the SVD [7] technique

TABLE II
EVALUATED ε_r USING THE PROPOSED VIE APPROACH FOR THE
PARALLEL-PLATE DR WITH $ra = 0$, $rb = 6.23$ mm, AND
 $L2 = 12.56$ mm. $L1 = L3 = 0$ FOR TYPE-I CONFIGURATION
AND $L1 = 0$ AND $L3 = 2.44$ mm FOR TYPE-II CONFIGURATION

	Type I Configuration		Type II Configuration	
	TE_{011} mode	TE_{012} mode	$TE_{01\delta}$ mode	$TE_{01(1+\delta)}$ mode
Measured f_0 (GHz)	7.7175	10.725	7.31	9.99
Ansoft-HFSS f_0 (GHz)	7.7541	10.7597	7.336	10.009
% diff. for f_0	0.474 %	0.324 %	0.356 %	0.19 %
ε_r (VIE approach)	9.5943	9.6133	9.6023	9.5997
Averaged ε_r	9.6024			
% diff. from $\varepsilon_{r,l}$	0.025 %			

was carried out for searching the ε_r value. In the iterative permittivity search using the TE_{011} or $TE_{01\delta}$ mode f_0 , $\Delta r' = rb/10$ and $\Delta z' = L2/10$. For the use of the TE_{012} or $TE_{01(1+\delta)}$ mode f_0 , $\Delta r' = rb/10$ and $\Delta z' = L2/20$. The obtained ε_r results and the measured f_0 are all presented in Table II. Approximately 0.025% difference is obtained as the averaged ε_r value is compared to the $\varepsilon_{r,1}$ value. A reverse check performed via Ansoft HFSS, which used the physical dimensions and the evaluated ε_r as input parameters to obtain the f_0 , is shown in the third row of Table II. Again, good agreement is observed, as comparison is made between the measured f_0 and simulated results.

The second example presents the evaluation of the $\tan \delta$ of a dielectric specimen using the proposed VIE formulation. The so-called ‘‘two-resonator method,’’ in which two resonators and two different resonant modes are used, is employed in the evaluation process [8]. The DR configuration considered in [8] implies that $L1 = L3 = 0$ since the analytical solution is available. However, [4] has indicated that much better accuracy can be obtained for the conditions such that $L1 > 0$ and $L3 > 0$, as the influence of the conductor losses on the Q factor of the resonant system can be reduced. Nevertheless, the parameters used in this example adopt those presented in [8] where the evaluated $\tan \delta$ is known for the sake of validation.

The matrix equation, which uses TE_{011} and TE_{014} modes in the evaluation of $\tan \delta$ for the dielectric specimen of interest and surface resistance (R_s) for the parallel-plate fixture, can be expressed as [2], [8]

$$\begin{bmatrix} \tan \delta \\ R_s \end{bmatrix} = \begin{bmatrix} 1 & B_{TE011} \\ 1 & B_{TE014} \end{bmatrix}^{-1} \begin{bmatrix} A_{TE011} \\ Q_{u,TE011} \\ A_{TE014} \\ Q_{u,TE014} \end{bmatrix} \quad (22)$$

where

$$A_{TE01l} = \left(1 + \frac{\int_{v'_{\text{free space}}} \left| \vec{E}_{TE01l}(\vec{R}) \right|^2 dv'}{\varepsilon_r \int_{v'_{\text{specimen}}} \left| \vec{E}_{TE01l}(\vec{R}) \right|^2 dv'} \right) \quad (23)$$

and

$$B_{TE01l} = \frac{\int_{s'_{\text{conductors}}} \left| \hat{a}_z \times \vec{H}_{TE01l}(\vec{R}) \right|^2 ds'}{\omega_0 \varepsilon_0 \varepsilon_r \int_{v'_{\text{specimen}}} \left| \vec{E}_{TE01l}(\vec{R}) \right|^2 dv'} \quad (24)$$

for $l = 1$ or 4 . As can be seen from (22)–(24), the evaluation of $\tan \delta$ and R_s requires the knowledge of $Q_{u,TE01l}$, ε_r , $\vec{E}_{TE01l}(\vec{R})$, and $\vec{H}_{TE01l}(\vec{R})$ at the resonant frequency (ω_0) of the TE_{01l} modes. While the $Q_{u,TE01l}$ can be extracted from the measurable $Q_{L,TE01l}$, the evaluation of ε_r from the measured ω_0 can be easily obtained via the SVD technique. In the permittivity search, $\Delta z' = L2/10$ and $\Delta z' = L2/40$ for the use of $f_{0,TE011}$ and $f_{0,TE014}$, respectively, while $\Delta r' = rb/10$ for both resonant modes. With the employment of (1), $\vec{E}_{TE01l}(\vec{R})$ in the dielectric specimen is readily obtained from the eigenvector of the eigenmatrix equation in (9). For the computation of $\vec{E}_{TE01l}(\vec{R})$ in the free-space region, the required formula is given in (A4). The space truncation boundary can be set approximately five times or even just three times the distance of rb , by which a good approximation can be achieved as fields decay exponentially away from the DR for those trapped resonant modes.

Evaluation of B_{TE01l} requires the computation of tangential $\vec{H}_{TE01l}(\vec{R})$ at the top and bottom conducting plates; hence, the magnetic PP DGF of the second kind $\vec{G}_{m2}(\vec{R}, \vec{R}')$, which relates the magnetic-field intensity $\vec{H}(\vec{R})$ due to the equivalent current density $\vec{J}_{\text{eq}}(\vec{R}')$, is needed. The required equation is

$$\begin{bmatrix} H_r \\ H_\phi \\ H_z \end{bmatrix} = \int_{v'} \begin{bmatrix} 0 & G_{m2,0}^{r\phi} & 0 \\ G_{m2,0}^{\phi r} & 0 & G_{m2,0}^{\phi z} \\ 0 & G_{m2,0}^{z\phi} & 0 \end{bmatrix} \cdot \begin{bmatrix} J_{\text{eq},r} \\ J_{\text{eq},\phi} \\ J_{\text{eq},z} \end{bmatrix} dv' \quad (25)$$

Since $J_{\text{eq},r} = J_{\text{eq},z} = 0$ in the analysis of the TE_{0nl} -mode family, the only equation of interest is the $H_r(\vec{R})$ component due to the nonzero $J_{\text{eq},\phi}(\vec{R}')$

$$H_r(\vec{R}) = \int_{v'} G_{m2,0}^{r\phi}(\vec{R}, \vec{R}') J_{\text{eq},\phi}(\vec{R}') dv' \quad (26)$$

where

$$\begin{aligned} G_{m2,0}^{r\phi}(\vec{R}, \vec{R}') &= \frac{-j}{2L} \cdot \sum_{m=1}^{\infty} \left(\left\{ \begin{array}{l} H_0^{(1)'}(k_r r) \cdot J_0'(k_r r') \\ J_0'(k_r r) \cdot H_0^{(1)'}(k_r r') \end{array} \right\} \right. \\ &\quad \left. \cdot k_z \cdot \cos(k_z z) \cdot \sin(k_z z') \right), \\ &\text{for } \begin{cases} r > r' \\ r < r' \end{cases}. \end{aligned} \quad (27)$$

TABLE III

COMPARISON OF VIE APPROACH WITH ANALYTICAL APPROACH [8] FOR THE EVALUATION OF $\tan \delta$ AND R_s . THE DR CONFIGURATION HAS $ra = L1 = L3 = 0$, $rb = 4.25$ mm, $L2_{TE011} = 3.572$ mm, AND $L2_{TE014} = 14.276$ mm. THE EXTRACTED $Q_{u,TE011} = 2237$, $Q_{u,TE014} = 4040$, AND THE MEASURED $f_{0,TE011} = f_{0,TE014} = 8.923$ GHz

Parameters	Analytical	Analytical	Proposed VIE	Proposed VIE
	TE_{011} mode	TE_{014} mode	TE_{011} mode	TE_{014} mode
ϵ_r	37.60	37.63	37.721	37.776
A_{TE01}	1.00262	1.00262	1.00255	1.00254
B_{TE01}	0.01028	0.00258	0.01042	0.00261
R_s (Ω)	2.60E-02		2.563E-02	
% diff. (R_s)	1.423 %			
$\tan \delta$	1.81E-04		1.8115E-04	
% diff. ($\tan \delta$)	0.0815 %			

The singularity in the numerical integration of (27) is treated in a similar manner as those five dyad components. The final expression for the self-coupling term evaluation of (26) after applying the singularity treatment is presented in (A7). With (1), (A4), (A7), measured f_0 and Q_u , $\tan \delta$ and R_s of the conducting plates can be easily obtained by solving the matrix equation in (22). Table III presents the computed numerical results in comparison with those using the analytical method presented in [8]. Good agreement is observed.

VI. CONCLUSION

An efficient VIE approach utilizing the PP-DGF kernel and VET has been presented for the characterization of the complex permittivity of a DR in the Courtney holder type of measurement environment. Computational efficiency for searching the permittivity is significantly increased as perturbation of the

eigenvalue matrix requires only recomputing a diagonal matrix that is a function of permittivity only. This attribute makes the approach very attractive for the evaluation of the complex permittivity from measured f_0 and Q_u values in an iteration process. Thanks to the novel singularity treatment that has been proposed in the paper, the inherent slow convergence behavior is overcome. Lossy rod and ring DRs have been analyzed to validate the correctness of the singularity treatments for all five dyad components. The proposed approach has been validated by the simulation results obtained from the FEM-based software Ansoft HFSS, the measurement conducted in-house, and the analytical solutions obtained from the literature. Good agreement has been observed in all cases.

APPENDIX

In general, the first step in extracting the singularity is to re-express the PP DGF as

$$\bar{\bar{G}}\left(\vec{R}, \vec{R}'\right) = \left\{ \bar{\bar{G}}\left(\vec{R}, \vec{R}'\right) - \bar{\bar{G}}_a\left(\vec{R}, \vec{R}'\right) \right\} + \bar{\bar{G}}_a\left(\vec{R}, \vec{R}'\right) \quad (\text{A1})$$

where $\bar{\bar{G}}_a(\vec{R}, \vec{R}')$ is the large argument Bessel function asymptotic representation of $\bar{\bar{G}}(\vec{R}, \vec{R}')$. The final expressions (before carrying out the inner product with the weighting function, i.e., ϕ -independent cylindrical Dirac delta function) for the self-coupling element evaluation of the six Green's function dyad components are presented here. While five dyad components ($\hat{r}\hat{r}$, $\hat{\phi}\hat{\phi}$, $\hat{r}\hat{z}$, $\hat{z}\hat{r}$, and $\hat{z}\hat{z}$) are due to the EFIE, one dyad component ($\hat{r}\hat{\phi}$) is due to (26).

For the $\hat{r}\hat{r}$ dyad component, see (A2), shown at the bottom of this page, where $F_2(r, z) = e^{-(\pi/L)r} \sin((\pi/L)z)$. z_{t1} , z_{t2} , z_{t3} , z_{t4} , and $F_1(r, z)$ have been specified in Section III.

$$\begin{aligned} & 2\pi \int_{z'_k - \frac{\Delta z'}{2}}^{z'_k + \frac{\Delta z'}{2}} \int_{r'_k - \frac{\Delta r'}{2}}^{r'_k + \frac{\Delta r'}{2}} G_{e1}^{rr}\left(\vec{R}, \vec{R}'\right) r' dr' dz' \\ &= \frac{j2\pi}{Lk_0^2} \sum_{m=1}^{\infty} \left\langle \left[\int_{r'_k - \frac{\Delta r'}{2}}^{r'_k + \frac{\Delta r'}{2}} \left\{ \begin{array}{l} H_0^{(1)'}(k_r r) J_0'(k_r r') \\ J_0'(k_r r) H_0^{(1)'}(k_r r') \end{array} \right\} r' dr' - \frac{2e^{j\frac{3}{4}\pi}}{j\pi k_z} \int_{r'_k - \frac{\Delta r'}{2}}^{r'_k + \frac{\Delta r'}{2}} \left\{ \begin{array}{l} e^{-k_z r} \cos\left(jk_z r' - \frac{3}{4}\pi\right) \\ \cos\left(jk_z r - \frac{3}{4}\pi\right) e^{-k_z r'} \end{array} \right\} \sqrt{\frac{r'}{r}} dr' \right] \right. \\ & \quad \cdot \left. \left[k_z \sin\left(k_z \frac{\Delta z'}{2}\right) \sin(k_z z) \sin(k_z z'_k) \right] \right\rangle, \quad \text{for } \begin{cases} r > r' \\ r < r' \end{cases} \\ & + \frac{1}{2Lk_0^2} \int_{r'_k - \frac{\Delta r'}{2}}^{r'_k + \frac{\Delta r'}{2}} \sqrt{\frac{r'}{r}} \left\langle e^{j\frac{3}{2}\pi} \left[\frac{F_2(r+r', z_{t2})}{F_1(r+r', z_{t2})} - \frac{F_2(r+r', z_{t1})}{F_1(r+r', z_{t1})} - \frac{F_2(r+r', z_{t3})}{F_1(r+r', z_{t3})} + \frac{F_2(r+r', z_{t4})}{F_1(r+r', z_{t4})} \right] \right. \\ & \quad \left. + \left[\frac{F_2(|r-r'|, z_{t2})}{F_1(|r-r'|, z_{t2})} - \frac{F_2(|r-r'|, z_{t1})}{F_1(|r-r'|, z_{t1})} - \frac{F_2(|r-r'|, z_{t3})}{F_1(|r-r'|, z_{t3})} + \frac{F_2(|r-r'|, z_{t4})}{F_1(|r-r'|, z_{t4})} \right] \right\rangle dr' \quad (\text{A2}) \end{aligned}$$

$$\begin{aligned}
 & 2\pi \int_{z'_k - \frac{\Delta z'}{2}}^{z'_k + \frac{\Delta z'}{2}} \int_{r'_k - \frac{\Delta r'}{2}}^{r'_k + \frac{\Delta r'}{2}} G_{e1,0}^{rz}(\vec{R}, \vec{R}') r' dr' dz' \\
 &= \frac{-j}{Lk_0^2} \frac{d}{dr} \sum_{m=1}^{\infty} \left\langle \left[\int_{r'_k - \frac{\Delta r'}{2}}^{r'_k + \frac{\Delta r'}{2}} \begin{Bmatrix} H_0^{(1)}(k_r r) J_0(k_r r') \\ J_0(k_r r) H_0^{(1)}(k_r r') \end{Bmatrix} r' dr' - \frac{2e^{j\frac{1}{4}\pi}}{j\pi k_z} \int_{r'_k - \frac{\Delta r'}{2}}^{r'_k + \frac{\Delta r'}{2}} \begin{Bmatrix} e^{-k_z r} \cos(jk_z r' - \frac{1}{4}\pi) \\ \cos(jk_z r - \frac{1}{4}\pi) e^{-k_z r'} \end{Bmatrix} \sqrt{\frac{r'}{r}} dr' \right] \right. \\
 & \quad \cdot \left. \left[\sin\left(k_z \frac{\Delta z}{2}\right) \sin(k_z z) \cos(k_z z') \right] \right\rangle, \quad \text{for } \begin{cases} r > r' \\ r < r' \end{cases} \\
 & + \frac{1}{4\pi k_0^2} \frac{d}{dr} \int_{r'_k - \frac{\Delta r'}{2}}^{r'_k + \frac{\Delta r'}{2}} \sqrt{\frac{r'}{r}} \left\langle e^{j\frac{1}{2}\pi} \ln \left[\frac{F_1(r+r', z_{t2}) \cdot F_1(r+r', z_{t3})}{F_1(r+r', z_{t1}) \cdot F_1(r+r', z_{t4})} \right] + \ln \left[\frac{F_1(|r-r'|, z_{t2}) \cdot F_1(|r-r'|, z_{t3})}{F_1(|r-r'|, z_{t1}) \cdot F_1(|r-r'|, z_{t4})} \right] \right\rangle dr' \quad (A3)
 \end{aligned}$$

$$\begin{aligned}
 & 2\pi \int_{z'_k - \frac{\Delta z'}{2}}^{z'_k + \frac{\Delta z'}{2}} \int_{r'_k - \frac{\Delta r'}{2}}^{r'_k + \frac{\Delta r'}{2}} G_{e1,0}^{zr}(\vec{R}, \vec{R}') r' dr' dz' \\
 &= \frac{j2\pi}{Lk_0^2} \left(\frac{d}{dr} + \frac{1}{r} \right) \sum_{m=1}^{\infty} \left\langle \left[\int_{r_k - \frac{\Delta r}{2}}^{r_k + \frac{\Delta r}{2}} \begin{Bmatrix} H_0^{(1)'}(k_r r) \\ J_0'(k_r r) \end{Bmatrix} \int_{r'_k - \frac{\Delta r'}{2}}^{r'_k + \frac{\Delta r'}{2}} \begin{Bmatrix} J_0'(k_r r') \\ H_0^{(1)'}(k_r r') \end{Bmatrix} r' dr' \right. \right. \\
 & \quad - \frac{2e^{-j\frac{3}{4}\pi}}{j\pi k_z} \left. \left. \begin{Bmatrix} e^{-k_z r} \\ \cos(jk_z r - \frac{3}{4}\pi) \end{Bmatrix} \int_{r'_k - \frac{\Delta r'}{2}}^{r'_k + \frac{\Delta r'}{2}} \begin{Bmatrix} \cos(jk_z r' - \frac{3}{4}\pi) \\ e^{-k_z r'} \end{Bmatrix} \sqrt{\frac{r'}{r}} dr' \right] \right. \\
 & \quad \cdot \left. \left[\sin\left(k_z \frac{\Delta z}{2}\right) \cos(k_z z) \sin(k_z z') \right] \right\rangle, \quad \text{for } \begin{cases} r > r' \\ r < r' \end{cases} \\
 & + \frac{-1}{4\pi k_0^2} \left(\frac{d}{dr} + \frac{1}{r} \right) \cdot \left(\int_{r_k - \frac{\Delta r}{2}}^{r_k + \frac{\Delta r}{2}} \sqrt{\frac{r'}{r}} \left\langle e^{-j\frac{3}{2}\pi} \log_e \left[\frac{F_2(|r+r'|, z_{t2}) \cdot F_2(|r+r'|, z_{t4})}{F_2(|r+r'|, z_{t1}) \cdot F_2(|r+r'|, z_{t3})} \right] \right. \right. \\
 & \quad \left. \left. + \log_e \left[\frac{F_2(|r-r'|, z_{t2}) \cdot F_2(|r-r'|, z_{t4})}{F_2(|r-r'|, z_{t1}) \cdot F_2(|r-r'|, z_{t3})} \right] \right\rangle dr' \right) \quad (A5)
 \end{aligned}$$

For the $\hat{r}\hat{z}$ dyad component, see (A3), shown at the top of this page.

For the $\hat{\phi}\hat{\phi}$ dyad component

$$2\pi \int_{z'_k - \frac{\Delta z'}{2}}^{z'_k + \frac{\Delta z'}{2}} \int_{r'_k - \frac{\Delta r'}{2}}^{r'_k + \frac{\Delta r'}{2}} G_{e1,0}^{\phi\phi}(\vec{R}, \vec{R}') r' dr' dz' \quad \cdot \frac{1}{k_z^2} \sin\left(k_z \frac{\Delta z}{2}\right) \sin(k_z z) \sin(k_z z') \left. \right\rangle, \quad \text{for } \begin{cases} r > r' \\ r < r' \end{cases}. \quad (A4)$$

For the $\hat{z}\hat{r}$ dyad component, see (A5), shown at the top of this page.

For the $\hat{z}\hat{z}$ dyad component, see (A6), shown at the top of the following page.

For the $\hat{r}\hat{\phi}$ dyad component of (26), see (A7), shown at the top of the following page.

$$\begin{aligned}
& 2\pi \int_{z'_k - \frac{\Delta z'}{2}}^{z'_k + \frac{\Delta z'}{2}} \int_{r'_k - \frac{\Delta r'}{2}}^{r'_k + \frac{\Delta r'}{2}} G_{e1,0}^{zz}(\vec{R}, \vec{R}') r' dr' dz' \\
&= \frac{j\pi\Delta z}{2L} \left[\left\{ \begin{array}{c} H_0^{(1)'}(k_0 r) \\ J_0(k_0 r) \end{array} \right\} \int_{r_k - \frac{\Delta r}{2}}^{r_k + \frac{\Delta r}{2}} \left\{ \begin{array}{c} J_0(k_r r') \\ H_0^{(1)}(k_r r') \end{array} \right\} r' dr' \right] \\
&+ \frac{j2\pi}{Lk_0^2} \sum_{m=1}^{\infty} \left\langle \left[\left\{ \begin{array}{c} H_0^{(1)}(k_r r) \\ J_0(k_r r) \end{array} \right\} \int_{r_k - \frac{\Delta r}{2}}^{r_k + \frac{\Delta r}{2}} \left\{ \begin{array}{c} J_0(k_r r) \\ H_0^{(1)}(k_r r) \end{array} \right\} r' dr' \right. \right. \\
&\quad \left. \left. - \frac{2e^{-j\frac{1}{4}\pi}}{j\pi k_z} \left\{ \begin{array}{c} e^{-k_z r} \\ \cos(jk_z r - \frac{1}{4}\pi) \end{array} \right\} \int_{r_k - \frac{\Delta r}{2}}^{r_k + \frac{\Delta r}{2}} \left\{ \begin{array}{c} \cos(jk_z r' - \frac{1}{4}\pi) \\ e^{-k_z r'} \end{array} \right\} \sqrt{\frac{r'}{r}} dr' \right] \right. \\
&\quad \left. \cdot \left[\frac{k_r^2}{k_z} \sin\left(k_z \frac{\Delta z}{2}\right) \cos(k_z z) \cos(k_z z') \right] \right\rangle, \quad \text{for } \begin{cases} r > r' \\ r < r' \end{cases} \\
&+ \frac{2}{Lk_0^2} \sum_{m=1}^{\infty} \left\langle \int_{r_k - \frac{\Delta r}{2}}^{r_k + \frac{\Delta r}{2}} \sqrt{\frac{r'}{r}} \left[e^{j\frac{1}{2}\pi} e^{-k_z|r+r'|} + e^{-k_z|r-r'|} \right] dr' \cdot \left[\frac{k_0^2}{k_z} \sin\left(k_z \frac{\Delta z}{2}\right) \cos(k_z z) \cos(k_z z') \right] \right\rangle \\
&+ \frac{1}{2Lk_0^2} \int_{r_k - \frac{\Delta r}{2}}^{r_k + \frac{\Delta r}{2}} \sqrt{\frac{r'}{r}} \left\langle e^{j\frac{1}{2}\pi} \left[\frac{F_1(|r+r'|, z_{t2})}{F_2(|r+r'|, z_{t2})} - \frac{F_1(|r+r'|, z_{t1})}{F_2(|r+r'|, z_{t1})} - \frac{F_1(|r+r'|, z_{t4})}{F_2(|r+r'|, z_{t4})} + \frac{F_1(|r+r'|, z_{t3})}{F_2(|r+r'|, z_{t3})} \right] \right. \\
&\quad \left. + \left[\frac{F_1(|r-r'|, z_{t2})}{F_2(|r-r'|, z_{t2})} - \frac{F_1(|r-r'|, z_{t1})}{F_2(|r-r'|, z_{t1})} - \frac{F_1(|r-r'|, z_{t4})}{F_2(|r-r'|, z_{t4})} + \frac{F_1(|r-r'|, z_{t3})}{F_2(|r-r'|, z_{t3})} \right] \right\rangle dr' \quad (\text{A6})
\end{aligned}$$

$$\begin{aligned}
& 2\pi \int_{z'_k - \frac{\Delta z'}{2}}^{z'_k + \frac{\Delta z'}{2}} \int_{r'_k - \frac{\Delta r'}{2}}^{r'_k + \frac{\Delta r'}{2}} G_{m2,0}^{z\phi}(\vec{R}, \vec{R}') r' dr' dz' \\
&= \frac{j2\pi}{L} \sum_{m=1}^{\infty} \left\langle \left[\int_{r_k - \frac{\Delta r}{2}}^{r_k + \frac{\Delta r}{2}} \left\{ \begin{array}{c} H_0^{(1)'}(k_r r) J_0'(k_r r') \\ J_0'(k_r r) H_0^{(1)}(k_r r') \end{array} \right\} - \frac{2e^{j\frac{3}{4}\pi}}{j\pi k_z \sqrt{rr'}} \int_{r_k - \frac{\Delta r}{2}}^{r_k + \frac{\Delta r}{2}} \left\{ \begin{array}{c} e^{-k_z r} \cos(jk_z r' - \frac{3}{4}\pi) \\ \cos(jk_z r - \frac{3}{4}\pi) e^{-k_z r'} \end{array} \right\} \right] r' dr' \right. \\
&\quad \left. \cdot \left(\sin\left(k_z \frac{\Delta z}{2}\right) \cos(k_z z) \sin(k_z z') \right) \right\rangle, \quad \text{for } \begin{cases} r > r' \\ r < r' \end{cases} \\
&+ \frac{-1}{4\pi} \left(\int_{r_k - \frac{\Delta r}{2}}^{r_k + \frac{\Delta r}{2}} \sqrt{\frac{r'}{r}} \left\langle e^{j\frac{3}{2}\pi} \log_e \left[\frac{F_1(|r+r'|, z_{t2}) \cdot F_1(|r+r'|, z_{t4})}{F_1(|r+r'|, z_{t1}) \cdot F_1(|r+r'|, z_{t3})} \right] + \log_e \left[\frac{F_1(|r-r'|, z_{t2}) \cdot F_1(|r-r'|, z_{t4})}{F_1(|r-r'|, z_{t1}) \cdot F_1(|r-r'|, z_{t3})} \right] \right\rangle dr' \right) \quad (\text{A7})
\end{aligned}$$

REFERENCES

- [1] D. Kajfez and P. Guillon, *Dielectric Resonators*, 2nd ed. Norwood, MA: Artech House, 1986.
- [2] B. W. Hakki and P. D. Coleman, "A dielectric resonator method of measuring inductive capacities in the millimeter range," *IRE Trans. Microwave Theory Tech.*, vol. MTT-8, pp. 402-410, July 1960.
- [3] W. E. Courtney, "Analysis and evaluation of a method of measuring the complex permittivity and permeability of microwave insulators," *IEEE Trans. Microwave Theory Tech.*, vol. MTT-18, pp. 476-485, Aug. 1970.
- [4] J. Krupka, "An accurate method for permittivity and loss tangent measurements of low dielectric using TE_{01δ}," in *5th Int. Dielectric Materials, Measurements Applications Conf.*, June 1988, pp. 322-325.

- [5] H. T. Hui and E. K. N. Yung, "Dyadic Green's functions for the inhomogeneous cylindrical waveguide and cavity and their applications," *J. Electromagn. Waves Applicat.*, vol. 11, pp. 1121–1138, 1997.
- [6] J. J. H. Wang, *Generalized Moment Methods in Electromagnetics: Formulation and Computer Solution of Integral Equations*. New York: Wiley, 1991.
- [7] V. A. Labay and J. Bornemann, "Matrix singular value decomposition for pole-free solutions of homogeneous matrix equations as applied to numerical modeling methods," *IEEE Microwave Guided Wave Lett.*, vol. 2, pp. 49–51, Feb. 1992.
- [8] Y. Kobayashi and M. Katoh, "Microwave measurement of dielectric properties of low-loss materials by the dielectric rod resonator method," *IEEE Trans. Microwave theory Tech.*, vol. MTT-33, pp. 586–592, July 1985.
- [9] M.-L. Lui and K.-L. Wu, "An efficient integral equation analysis for characterizing lossy dielectric resonator," in *IEEE MTT-S Int. Microwave Symp. Dig.*, pp. 1835–1838.



Man-Leung Lui (S'04) received the B.Eng. and M.A.Sc. degrees from Dalhousie University, Halifax, NS, Canada, in 1996 and 1999, respectively, and is currently working toward the Ph.D. degree in electronic engineering from The Chinese University of Hong Kong, Shatin, Hong Kong.

From 1996 to 1999, he was a Research Assistant with the Microwave and Wireless Research Laboratory, Department of Electrical and Computing Engineering, DalTech, Dalhousie University. His current research interests include numerical modeling of passive structures, integral-equation techniques, and material characterization.



Ke-Li Wu (M'90–SM'96) received the B.S. and M.Eng. degrees from the Nanjing University of Science and Technology, Nanjing, China, in 1982 and 1985, respectively, and the Ph.D. degree from Laval University, Quebec, QC, Canada, in 1989.

From 1989 to 1993, he was with the Communications Research Laboratory, McMaster University, Hamilton, ON, Canada. In March 1993, he joined the Corporate Research and Development Division, Com Dev International, where he had been a Principal Member of Technical Staff in charge of developing advanced EM design software for various microwave subsystems. Since October 1999, he has been with the Department of Electronic Engineering, The Chinese University of Hong Kong, Shatin, Hong Kong, where he is a Professor. He has authored or coauthored numerous publications in the areas of electromagnetic (EM) modeling and microwave and antenna engineering. He contributed to *Finite Element and Finite Difference Methods in Electromagnetics Scattering* (Amsterdam: The Netherlands: Elsevier, 1990) and *Computational Electromagnetics* (Amsterdam, The Netherlands; Elsevier, 1991). He holds two patents. His current research interests include all the aspects related to low-temperature co-fired ceramic (LTCC) multichip modules (MCMs) from EM modeling to design methodology and various applications.

Dr. Wu was a recipient of the 1992 URSI Young Scientist Award and the 1998 Com Dev Achievement Award.